Applied Catalysis A: General 391 (2011) 367–376

Contents lists available at ScienceDirect

Applied Catalysis A: General

journal homepage: www.elsevier.com/locate/apcata

XPS characterization of Au/TiO_2 catalysts: Binding energy assessment and irradiation effects

Norbert Kruse*, Sergey Chenakin[1]

Université Libre de Bruxelles (ULB), Chimie-Physique des Matériaux, CP243 Campus Plaine, B-1050 Bruxelles, Belgium

ARTICLE INFO

Article history:
Received 15 February 2010
Received in revised form 14 May 2010
Accepted 26 May 2010
Available online 4 June 2010

Keywords:
Au/TiO_2 catalyst
TiO_2
XPS
X-ray induced damage
Valence band

ABSTRACT

X-ray photoelectron spectroscopy (XPS) was employed to study the surface composition and electronic structure of Au/TiO_2 catalysts in comparison with TiO_2 (anatase) and to reveal time-dependent X-ray irradiation damage of the samples. The occurrence of Au nano-sized particles on a TiO_2 support was found to result in a slight shift of Ti 2p core-level spectrum and in changes of the valence band and X-ray induced Auger spectra, compared to TiO_2-only. It was shown that for different means of energy referencing the charge-corrected Au $4f_{7/2}$ binding energy in Au/TiO_2 catalysts was 0.15–0.45 eV lower than that in pure bulk Au. Exposure to X-rays of Au/TiO_2 catalysts and pure TiO_2 caused a reduction of Ti 4+ oxidation state and desorption of oxygen from the surface. As a result, the surface chemical composition and electronic structure of the samples changed with time. The X-ray irradiation affected charge transfer processes in Au/TiO_2 so that the pattern of X-ray induced damage in the Au-based catalyst turned out to be quite different from that in TiO_2, with some characteristics displaying the very opposite features. Decreasing of the Au $4f_{7/2}$ binding energy and concurrent increasing of the fraction of Ti^{3+} species observed in the beginning of X-ray irradiation of Au/TiO_2 may be taken as direct evidence for charge transfer from oxygen vacancies created by irradiation to Au particles.

1. Introduction

X-ray photoelectron spectroscopy (XPS) is being widely used to provide valuable information on the chemical composition and electronic structure of catalyst surfaces. Analysis of these characteristics as a function of preparation and reaction conditions is very helpful in understanding and improving the catalysts' performance, and in developing new catalytic systems. Lab-size XPS equipment allows an independent and fast characterization of catalyst materials. The time factor might be rather crucial in screening procedures where chemical surface composition can vary as a function of preparation recipes and catalyst conditioning.

XPS is generally considered to be an essentially non-destructive technique. However certain metal salts and organometallic compounds used as catalyst precursors may decompose during XPS analysis. For a general introduction into the matter, see ref. [1]. Moreover, some metal oxides considered to be important in catalysis may suffer X-ray irradiation induced reduction [2,3]. Recently, we have shown that the XPS analysis of oxide-containing catalysts requires great care inasmuch as considerable damage may already be encountered at low X-ray doses [4,5]. No similar study on Au/TiO_2 catalysts seems to be available at present, which is surprising since these catalysts are most active in the low-temperature CO oxidation and presently define a benchmark system. On the other hand, XPS has been used quite extensively to determine the influence of the following: preparation method [6–9]; precipitation pH [10]; drying pretreatment [11]; conditioning [8,9,12,13]; calcination temperature [14–17]; Au loading [12,14,16,17]; Au cluster size/morphology [18–23]; conditions and time of storage of the catalyst [24,25]; nature of the support [7,8,21,22,26]; titania support morphology [27]; acid-base treatment of the titania support [24]; loading of TiO_2 with MnO_2 [10]; incorporation of impurities [28]; CO adsorption [29]; and catalytic reaction conditions [6,14,15,26,30,31] on surface composition and gold chemical and electronic state in the catalyst. X-ray absorption spectroscopy methods (XANES and EXAFS) are also being widely employed to characterize the structure and oxidation state of gold in the Au/TiO_2 catalysts under different preparation and reaction conditions [13,32,33]. Although X-rays were suspected to cause reduction of cationic gold species in XPS [6] and XAS studies [33], only Schumacher et al. [11] reported that their XPS spectra were recorded rather quickly to avoid radiation-induced changes of the Au/TiO_2 catalyst composition, especially for as-prepared and dried samples. In fact, while characterizing dried Au/TiO_2 samples by XPS, Zanella and Louis [34] have observed a significant X-ray induced reduction of what they argue to be an Au^{3+} state in Au/TiO_2. Yang et

* Corresponding author. Tel.: +32 2 6505714; fax: +32 2 6505708.
E-mail address: nkruse@ulb.ac.be (N. Kruse).
[1] Permanent address: Institute of Metal Physics, Nat. Acad. Sci., Akad. Vernadsky Blvd. 36, 03680 Kiev-142, Ukraine.

0926-860X/$ – see front matter © 2010 Elsevier B.V. All rights reserved.
doi:10.1016/j.apcata.2010.05.039

al. [13] found that the exposure of an as-prepared Au/TiO_2 catalyst to an X-ray beam in XAS measurements had no noticeable effect; however, X-ray irradiation caused a detectable further reduction in the sample which had previously been partially reduced. Employing XPS, Dalacu et al. [21] have noted that binding energy and half-width of the Au $4f_{7/2}$ spectra of Au particles as deposited on SiO_2 in a range of concentrations were sensitive to the X-ray irradiation, and that at higher X-ray flux they corresponded to those of the annealed Au/SiO_2 samples, which was attributed to local heating of the samples by the irradiation.

The aim of the present work is to provide a comprehensive XPS characterization of a supported Au/TiO_2 catalyst and to systematically study the effect of X-rays on the material. To do so, we have selected the Au/TiO_2 World Gold Council (WGC) standard which is widely used in research in many laboratories. The question for X-ray induced structural and electronic alterations is inherently related to a careful analysis of binding energy shifts. We therefore started by addressing this issue first, and discussing the problems encountered in setting the binding energy scale. For the purposes of comparison, the behavior of a reference oxide TiO_2 (anatase) during extended exposure to X-rays was also investigated. Various features of the XPS spectra were evaluated to allow the surface composition and electronic structure of the samples to be followed as a function of time of exposure to X-rays.

2. Experimental

An Au/TiO_2 gold reference catalyst prepared by deposition–precipitation and provided by the World Gold Council (Lot No. 02-4, sample 23A) was investigated. According to the certificate, the Au loading in the Au/TiO_2 WGC standard was 1.51 wt.% (ICP) and the average Au particle diameter 3.8 nm (TEM). In the CO oxidation studies performed for the WGC catalyst with a 2% CO + 2% O_2 (Ar balance) gas mixture at room temperature for 1 h, a stable CO to CO_2 conversion of 91% was obtained.

Commercial TiO_2 anatase powder (Rhone-Poulenc-CRA), calcined at 600 °C for 2 h, was studied for comparison. Both Au/TiO_2 and TiO_2 powder samples were pressed uniformly over an indium film on a flat sample holder so as to form a layer suitable for XPS analysis, about 0.1 mm thick.

Experiments were performed in a combined XPS–ToF-SIMS instrument at a base pressure of 1.4×10^{-9} mbar. A non-monochromatic Mg K_α radiation was used at an operating power of 15 kV × 10 mA. Prior to analysis, the samples were outgassed for 220 h in a preparation chamber at a base pressure of 5×10^{-10} mbar. Photoelectron core-level spectra were acquired using a hemispherical analyzer at a pass-energy of 50 eV with a 0.05 eV energy step. The overall resolution of the spectrometer in this operating mode was 0.96 eV measured as a full width at half maximum (FWHM) of the Ag $3d_{5/2}$ line. The spectrometer was calibrated against E_B (Au $4f_{7/2}$) = 84.0 eV. Spectra were measured at room temperature as a function of time of exposure to X-rays during continuous irradiation of the samples for 3 h. Acquisition of core-level spectra (in a sequence: Ti 2p, O 1s, Au 4f, C 1s, O 2s + Ti 3p) was started immediately after the sample was moved under the running X-ray source. The first spectrum acquired was defined as the "virgin state" at "zero-time" X-ray exposure. The acquisition time of the first Ti 2p spectrum was 44 s. In addition, the O $KL_{23}L_{23}$ and Ti LMV Auger lines and valence band spectra were recorded at "zero-time" and at the end (2.5 h exposure) of the measurements. After subtraction of the Shirley-type background, the core-level spectra were decomposed into their components with mixed Gaussian–Lorentzian lines by a non-linear least squares curve-fitting procedure, using the public software package XPSPEAK 4.1. The binding energies (E_B) and FWHM of the peaks were determined from the fitting results. Deconvoluted peak areas and standard sensitivity factors [35] were used to evaluate the surface composition of the samples. The carbon C 1s line at 284.8 eV was taken as a reference for surface-charging corrections. As a reference for bulk metallic Au, core-level and valence band spectra were recorded from a pure Au foil, sputter-cleaned with 500 eV Ar^+ ions for 15 min.

XPS measurements as a function of the X-ray irradiation dose were performed for each sample in two series and the patterns were found to be reproducible. The release of gaseous components into the residual atmosphere during X-ray irradiation of the samples was studied with a quadrupole mass spectrometer (Hiden Analytical). Ion peaks of m/e = 1, 2, 14, 16, 18, 28, 32, and 44 were continuously monitored with a time increment of 5 s.

3. Results

3.1. XPS core-level analysis of Au/TiO_2 WGC catalyst and TiO_2

Fig. 1 shows the Ti 2p, O 1s, C 1s and Au 4f as-measured spectra of the Au/TiO_2 WGC catalyst taken at "zero-time" X-ray exposure. The Ti 2p, O 1s and C 1s core-level spectra of intact reference oxide TiO_2 are similar to those of Au/TiO_2. According to the deconvolution results, the Ti 2p spectrum of WGC catalyst is dominated by species in the Ti^{4+} oxidation state with the presence of a small contribution of reduced species Ti^{3+} (Fig. 1(a)), which appears at a binding energy of ~2.3 eV below the Ti^{4+} peak with a fractional amount of ~3.6%. The reduced Ti^{3+} species was also observed in studies with annealed

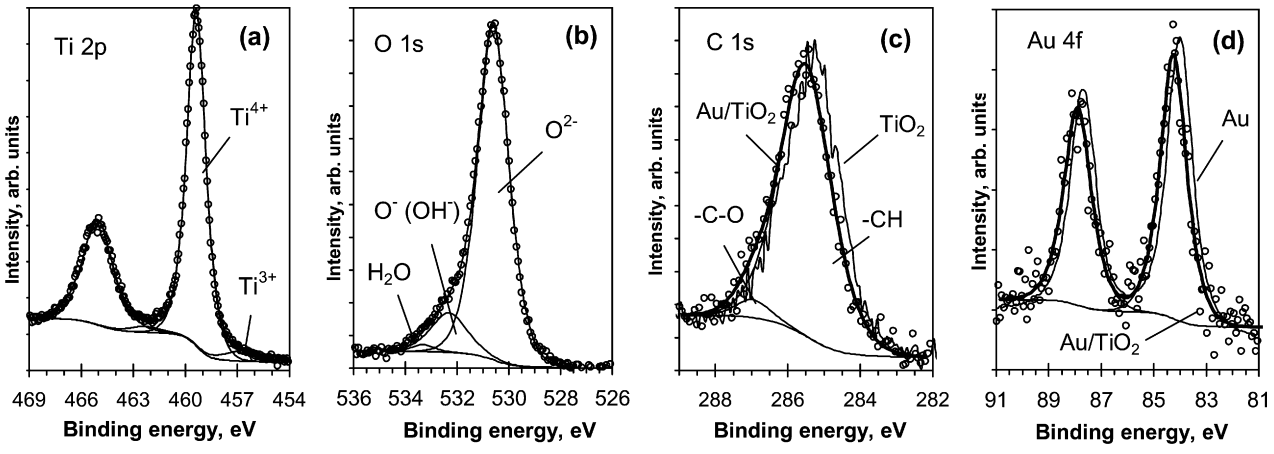

Fig. 1. Curve-fitted as-measured (a) Ti 2p, (b) O 1s, (c) C 1s, and (d) Au 4f XP core-level spectra for Au/TiO_2 catalyst. The C 1s spectrum without curve fitting for reference TiO_2 anatase (c) and Au 4f spectrum for pure Au foil (d) are also shown. No correction of binding energy scale for charge effects is applied.

Au film on TiO_2 [36] and with Au particles on TiO_2 [19,29]. In the Ti 2p spectrum of the reference TiO_2, a reduced species Ti^{3+} can be seen at a binding energy of ~2.1 eV below the Ti^{4+} peak, and its fractional amount is about 3.9%.

The O 1s spectrum (Fig. 1(b)) is asymmetrical, with a tail extending towards higher energies. A similar shape was previously observed for the Au/TiO_2 catalyst prepared by deposition–precipitation [12] and magnetron sputtering [24], for TiO_2 anatase powder [37,38], anatase single crystal [39] and nanocrystalline film [40], and also for rutile TiO_2 [41]. Tentatively, the O 1s line in TiO_2 was considered as being composed of two [41] or three components [39]. While the presence of O^{2-} species is unequivocal, the assignment of the other components is not as clear. In the two-component approach, the minor component forming the high-energy tail (shoulder) and appearing at about 1.6–1.9 eV above the major O^{2-} peak of the O 1s line was attributed either to the presence of a weakly adsorbed species and/or subsurface low-coordinated oxygen ions O^- [41]; or, alternatively, to surface hydroxyl OH and/or carbonate species [12,38,40]. In the three-component approach, the high-energy tail was assumed to be caused by two minor species assigned to hydroxyl groups and adsorbed water molecules respectively [37–39,42]. It was also brought to our attention [42] that organic carbon contaminations containing C–O, O–C=O groups and –COOH acidic function may fall close to OH and H_2O peak locations respectively. Components associated with OH groups may also be influenced by oxygen vacancies created by thermal treatment [39] or sputtering [42].

We have analyzed our O 1s spectra in terms of both two- and three-component deconvolution and found that the energy separation between OII (O^-, OH species) and OI (O^{2-} species) peaks in the O 1s spectrum of the Au/TiO_2 WGC catalyst is relatively high. The two-component fitting yields a value $\Delta E_B = 1.77$ eV ($\Delta E_B = 1.63$ eV for a three-component fitting) which is 0.13 eV (0.37 eV) larger than that for reference oxide TiO_2. This larger energy separation (OII–OI) may be related to the structure and phase composition of the support. Accordingly, titania (P25 Degussa) used as the support in the WGC reference catalyst typically comprises 75 ± 5 wt.% anatase and 25 ± 5 wt.% rutile, with the content of the latter being dependent on the calcination conditions [43]. The different crystalline structure, crystal size and surface area of the anatase and rutile components may affect the adsorption of water and the formation of hydroxyl groups [44]. In fact, for an in-house Au/TiO_2 catalyst prepared by deposition–precipitation of gold onto a home-made anatase precursor [45], we observed nearly the same separation ΔE_B (OII–OI) in the O 1s spectrum as for the commercial anatase powder. The opposite trend was observed [24] for Au/TiO_2 (P25) catalysts prepared by magnetron sputtering, for which the separation ΔE_B (OII–OI) was smaller (1.44–1.59 eV) than that of the original or treated TiO_2 (P25) (1.73 eV).

The atomic ratio $O^{2-}/Ti^{4+} = 2.12$ in the Au/TiO_2 WGC catalyst appears to be larger than the stoichiometric ratio $O^{2-}/Ti^{4+} = 2.03$ in TiO_2, while the ratios O_{tot}/Ti_{tot} in both samples are about the same (2.37 and 2.39 respectively), and are close to literature data [12].

The C 1s spectrum of the Au/TiO_2 WGC catalyst (Fig. 1(c)) is dominated by C–H/C–C species and is slightly asymmetrical due to the contribution of C–O groups (~7%) [42]. The as-measured C 1s peak position indicates some charging of the sample (compared to the reference at 284.8 eV). In the WGC catalyst, the C 1s line is found to be shifted to higher E_B by ~0.27 eV with respect to that in TiO_2-only; besides, its shape turns out to be different from that of TiO_2 (Fig. 1(c)).

Fitting the Au 4f spectrum of the Au/TiO_2 WGC catalyst (Fig. 1(d)) shows gold nanoparticles to be in a single metallic state. The amount of gold on the catalyst is evaluated to be ~0.78 at.% and the atomic ratio Au/Ti ~0.027. For comparison, Fig. 1(d) also shows the Au 4f spectrum of the pure Au foil. As a result of surface charging, the as-measured Au 4f spectrum of Au/TiO_2 is seen to be shifted to higher binding energies with respect to that of Au foil. The charging effects and referencing problem will be considered later.

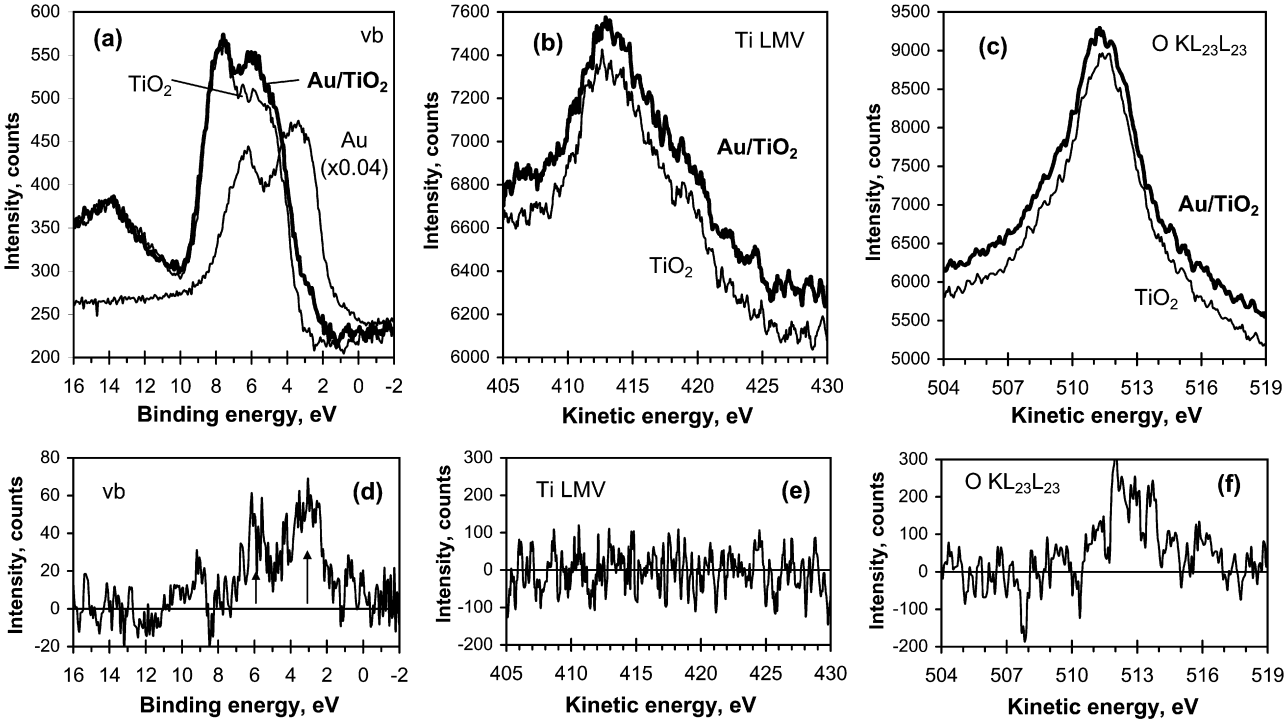

Fig. 2. Upper panel: (a) valence band and X-ray induced (b) Ti LMV and (c) O $KL_{23}L_{23}$ Auger spectra for anatase TiO_2 and Au/TiO_2 catalyst. For comparison, in (a), the valence band of pure bulk Au is presented. For the sake of clarity, the spectra are spaced apart along the *y*-axis. Lower panel: the difference spectra between (d) valence bands, (e) Ti LMV and (f) O $KL_{23}L_{23}$ Auger lines of Au/TiO_2 and TiO_2. No correction of binding energy scale for charge effects is applied.

3.2. XPS valence band and Auger spectra of Au/TiO_2 WGC catalyst and TiO_2

The valence band of TiO_2 (Fig. 2(a)) with a band gap of ~3 eV is characterized by two broad peaks at ~5.8 and ~7.6 eV related mainly to non-bonding and bonding O 2p orbitals respectively. The parameters of the valence band are consistent with published data for anatase [39,40]. As compared to TiO_2, the valence band of the Au/TiO_2 WGC catalyst (Fig. 2(a)) reveals the intensity to be enhanced in regions centered at ~3 eV and ~6 eV. This is clearly seen in the difference spectrum (Fig. 2(d): the regions of intensity enhancement are indicated by arrows). Note that the difference spectrum bears strong resemblance to the valence band of pure Au foil (Fig. 2(a)), thus proving that the increase of the intensity in these regions is largely due to the Au 5d bands. A progressive growth of intensity at these binding energies corresponding to the Au 5d states was also observed [46] in the valence band of TiO_2 (1 1 0) upon deposition of increasing amounts of gold.

Fig. 2(b) shows Ti LMV peaks in TiO_2 and Au/TiO_2 WGC. The shape of the Ti LMV ($L_{23}M_{23}M_{45}$) Auger line was shown [47] to be related to the stoichiometry of titanium oxides and associated with the valence band profile (since valence electrons are involved in the LMV Auger transition). In fact, the shape of the peaks in the kinetic energy region of 411–416 eV closely resembles the intense part of the valence band ~5 eV wide. Despite some distinctions in the valence band profile of TiO_2 and Au/TiO_2 (Fig. 2(a)) there is no difference between the Ti LMV lines for the two samples (Fig. 2(e)). This may mean that the Au 5d states do not participate in the Ti LMV Auger transitions; the Auger decay seems to involve only Ti 3d electronic states of the valence band of Au/TiO_2 which are not affected by the presence of gold. The O KVV (O $KL_{23}L_{23}$) Auger transitions also involve electrons from the valence band. In contrast to Ti LMV, however, the O KVV Auger peaks for TiO_2 and Au/TiO_2 (Fig. 2(c)) exhibit some dissimilarity. The difference spectrum (Fig. 2(f)) demonstrates an intensity enhancement in the kinetic energy region 511–514 eV, which implies that the valence band of Au/TiO_2 has a higher density of non-bonding O 2p states than TiO_2 and/or that the Au 5d states partly contribute to the O KVV decay.

Using the O 1s, Ti $2p_{3/2}$ peaks and O KVV, Ti LMV Auger lines, modified Auger parameters α' (=binding energy of photoelectron peak + kinetic energy of Auger peak) for oxygen and titanium can be determined. In TiO_2, we obtain $\alpha'(O) = 1042.2$ eV and $\alpha'(Ti) = 872.9$ eV which are close to the literature values [48]. In Au/TiO_2, $\alpha'(O) = 1042.1$ eV and $\alpha'(Ti) = 872.6$ eV.

3.3. Extended exposure to X-rays: Au/TiO_2 WGC catalyst and TiO_2

To reveal the influence of extended X-ray irradiation on the surface physico-chemical state of TiO_2 and Au/TiO_2, we measured various XPS characteristics as a function of the time of exposure. Generally, the quantitative evaluation of the core-level spectra (E_B, FWHM and fraction of a particular component) is dependent on the way the deconvolution is done (number of used components, type of constraints). We present only those results which show, qualitatively, the same trends, whatever the deconvolution procedure. For various methods of the spectra deconvolution, the standard deviation of the E_B and FWHM values at a given X-ray exposure did not exceed 0.02 eV and 0.04 eV respectively.

Continuous exposure to X-rays of TiO_2 and the Au/TiO_2 WGC catalyst causes the Ti $2p_{3/2}$ peak (Ti^{4+} component) to gradually broaden. Fig. 3(a) shows that the Ti^{4+} FWHM increases in both samples in a similar manner. FWHM of the O 1s peak (O^{2-} species) in

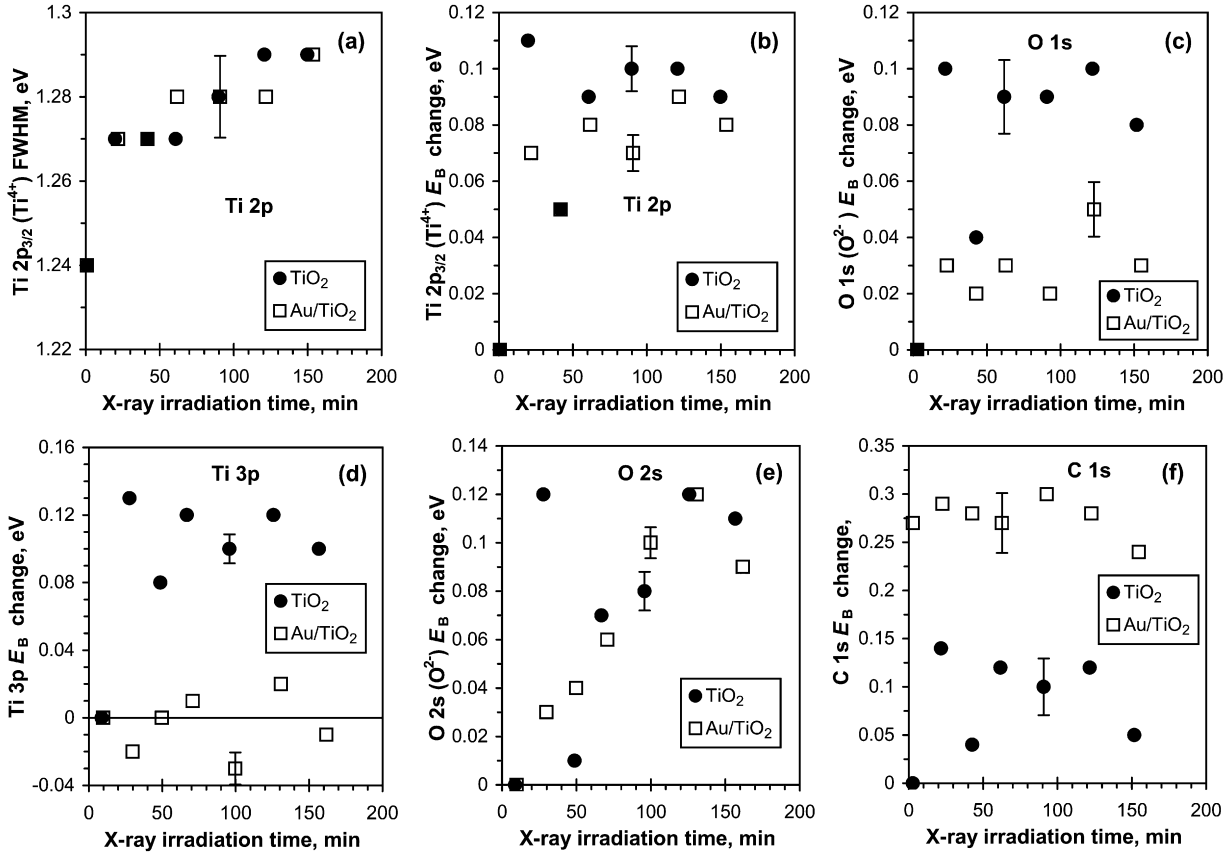

Fig. 3. X-ray induced changes in core-level spectra of anatase TiO_2 (filled circles) and Au/TiO_2 catalyst (squares): (a) FWHM of the Ti $2p_{3/2}$ line (Ti^{4+} species) and relative change of as-measured binding energy of the (b) Ti $2p_{3/2}$ (Ti^{4+} species), (c) O 1s (O^{2-} species), (d) Ti 3p, (e) O 2s (O^{2-} species) and (f) C 1s (C–H species) photoelectrons as a function of X-ray exposure.

the samples experiences negligible changes. During X-ray irradiation the Ti $2p_{3/2}$ and O 1s binding energies increase. While the Ti $2p_{3/2}$ E_B changes similarly in both TiO_2 and Au/TiO_2 (Fig. 3(b)), the shift of the O^{2-} component in the Au-containing catalyst is noticeably smaller than in TiO_2 (Fig. 3(c)). It is also worth noting that the binding energies of the Ti 3p (Fig. 3(d)) and O 2s (Fig. 3(e)) photoelectrons in Au/TiO_2 vary differently from the E_B of the respective Ti 2p and O 1s photoelectrons. Finally, Fig. 3(f) shows the X-ray induced variation of the C 1s binding energy in TiO_2 and WGC catalyst plotted relative to the original C 1s E_B value in virgin TiO_2 to underline the noticeable initial difference in the C 1s E_B of the two samples. Several noteworthy features are seen: (i) exposure of TiO_2 to X-rays causes a noticeable increase in the binding energy (by about 0.15 eV) at the very beginning of X-ray irradiation; (ii) on the contrary, the C 1s E_B in Au/TiO_2 is influenced by X-ray irradiation in a minor way; (iii) the initial C 1s E_B in WGC is higher than that in TiO_2 (see Fig. 1(c)) and this difference is retained over the whole period of X-ray exposure; (iv) for TiO_2, the scatter of Ti $2p_{3/2}$ (Fig. 3(b)), Ti 3p (Fig. 3(d)), O 1s (Fig. 3(c)) and O 2s (Fig. 3(e)) binding energies follows the scatter of C 1s E_B (Fig. 3(f)), thus indicating that charging effects in this sample play a major role.

The binding energies of the Ti^{4+} and O^{2-} components in TiO_2 and the WGC catalyst were corrected for charging effects using the C 1s line in the respective samples. By plotting the change of the charge-corrected binding energies in the given X-irradiated sample, relative to the corrected E_B of this sample in the original state ("zero time exposure"), we can eliminate the substrate dependence of the C 1s line and thus compare trends for TiO_2 and Au/TiO_2. As can be seen in Fig. 4(a), in TiO_2 the correct Ti $2p_{3/2}$ binding energy (Ti^{4+} species) practically does not change during extended X-ray irradiation. Note that the corrected E_B of the Ti 3p photoelectrons (Fig. 4(b)) originating from deeper layers of TiO_2 behaves in the same way. In Au/TiO_2 however, completely different trends are observed for the corrected binding energies: while E_B of Ti $2p_{3/2}$ rises monotonically (Fig. 4(a)), the Ti 3p line position is practically unaffected (Fig. 4(b)). The corrected binding energy of O^{2-} species derived from the O 1s peak (Fig. 4(c)) demonstrates in both samples minor changes. The corrected O 2s E_B (Fig. 4(d)), however, changes somewhat differently from the O 1s E_B, demonstrating a slight variation in TiO_2 and a stronger monotonic rise in Au/TiO_2 (cf. Fig. 4(c)).

A noteworthy feature of the above results is the quite different variation of the corrected binding energies under X-ray irradiation in TiO_2 and Au/TiO_2. To verify the derived trends, it would be reasonable to modify the calibration procedure. Fig. 4 shows that, as distinct from Ti 2p, O 1s and O 2s, the binding energy of the Ti 3p photoelectrons remains practically unaffected by enduring X-ray irradiation in both TiO_2 and Au/TiO_2. In view of this remarkable fact, the Ti 3p line appears to be a good reference for correcting the charge effects in these samples. In Fig. 5(a) and (b) we present the binding energies of the Ti 2p (Ti^{4+}) and O 1s (O^{2-}) core levels corrected by referencing the Ti 3p peak to E_B = 37.5 eV reported for TiO_2 [49]. One can see that (i) the Ti 2p correct binding energy in intact Au/TiO_2 turns out to be about 0.12 eV lower than that in TiO_2; (ii) during the course of X-ray irradiation the Ti 2p E_B in Au/TiO_2 increases monotonically and after 70–90 min of irradiation approaches the value for TiO_2; and (iii) the Ti 2p, O 1s E_B in TiO_2 and O 1s E_B in Au/TiO_2 display minor variations under irradiation.

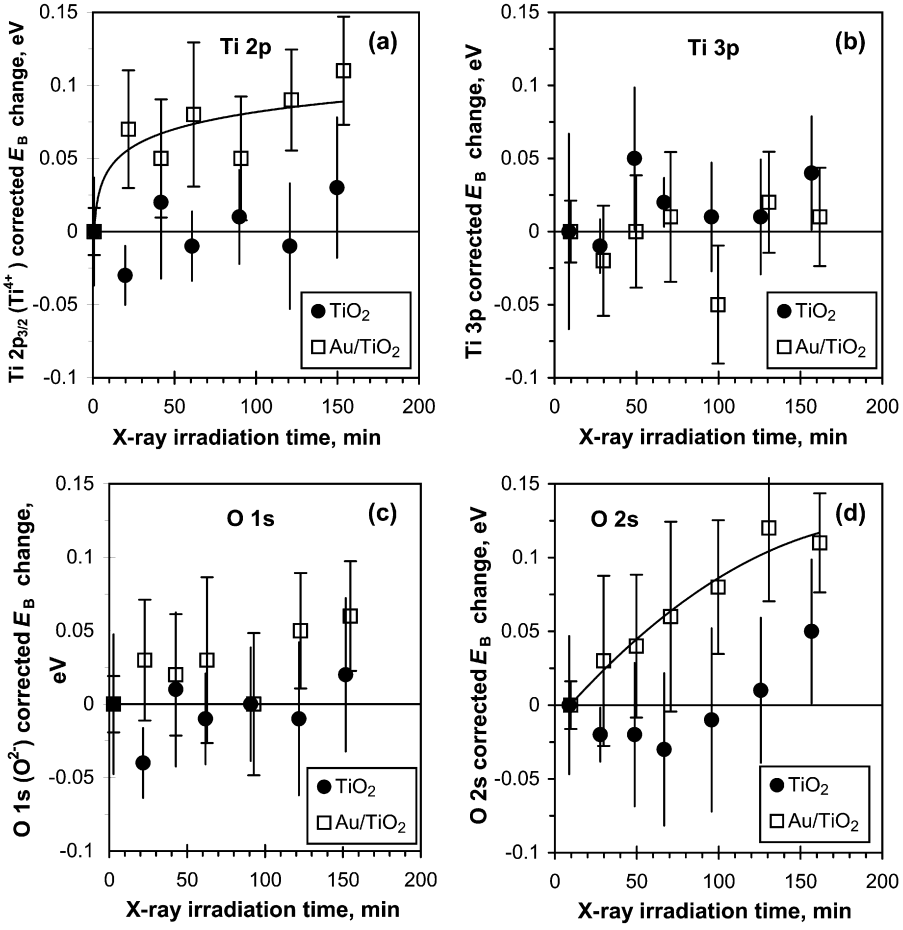

Fig. 4. Relative change of the (a) Ti $2p_{3/2}$ (Ti^{4+} species), (b) Ti 3p, (c) O 1s (O^{2-} species), and (d) O 2s binding energies, which were charge-corrected using C 1s reference line, as a function of X-ray irradiation time for anatase TiO_2 (filled circles) and Au/TiO_2 catalyst (squares). The polynomial trend lines are drawn to guide the eye.

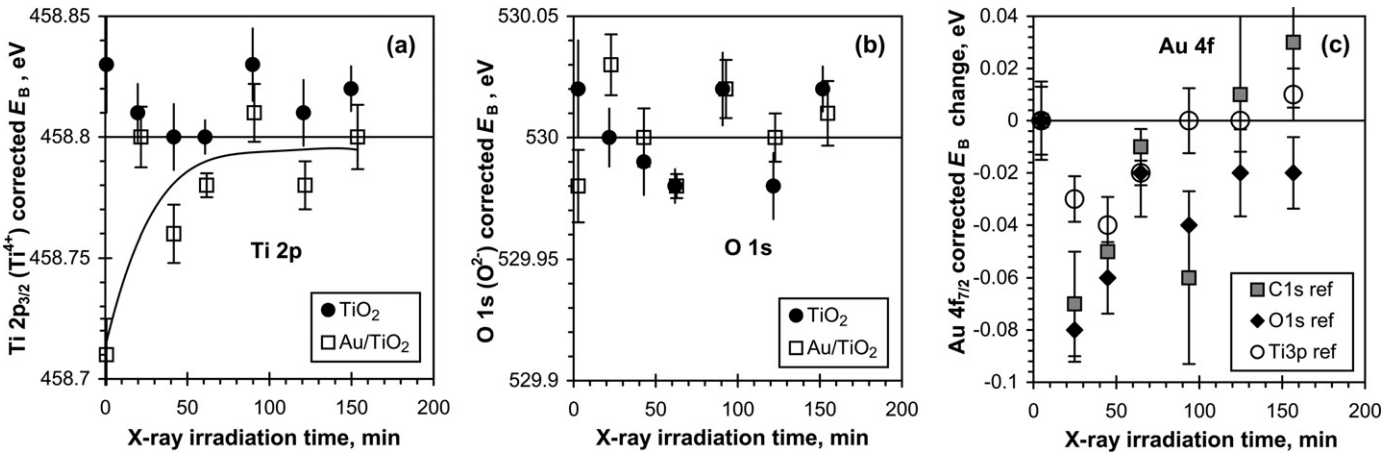

Fig. 5. (a) Ti $2p_{3/2}$ (Ti^{4+}) and (b) O 1s (O^{2-}) binding energies corrected for surface charging using Ti 3p reference line for anatase TiO_2 (filled circles) and Au/TiO_2 catalyst (squares) as a function of X-ray exposure; (c) relative change of the Au $4f_{7/2}$ binding energy under X-ray irradiation of Au/TiO_2 with the charge correction using C 1s, O 1s and Ti 3p references. The polynomial trend line is drawn for the Ti 2p E_B to guide the eye.

Accordingly, taking the C 1s, Ti 3p and O 1s (at $E_B = 530$ eV reported for TiO_2 [39,41]) lines as a reference for charge correction, we derived the Au $4f_{7/2}$ binding energies in the WGC catalyst, which are plotted in Fig. 5(c) as a function of X-ray exposure relative to the Au $4f_{7/2}$ E_B in the intact sample. The corrected Au $4f_{7/2}$ E_B is seen to change non-monotonically and exhibits a steep drop of about 0.07–0.08 eV (for C 1s and O 1s referencing) at the beginning of X-ray irradiation followed by a gradual rise later on. A similar decrease in the Au $4f_{7/2}$ E_B was also observed for the in-house Au/TiO_2 catalyst exposed to X-rays for about 30 min. In contrast to the Ti $2p_{3/2}$ and O 1s lines (Fig. 3(a)), the FWHM of the Au $4f_{7/2}$ peak slightly decreases under X-ray irradiation (by about 5%) but still remains above the value for bulk Au (1.12 eV).

Besides changes in the E_B and FWHM of the photoelectron lines, X-ray induced compositional modifications are also observed (Figs. 6). The fraction of reduced titanium species (Ti^{3+}) originally

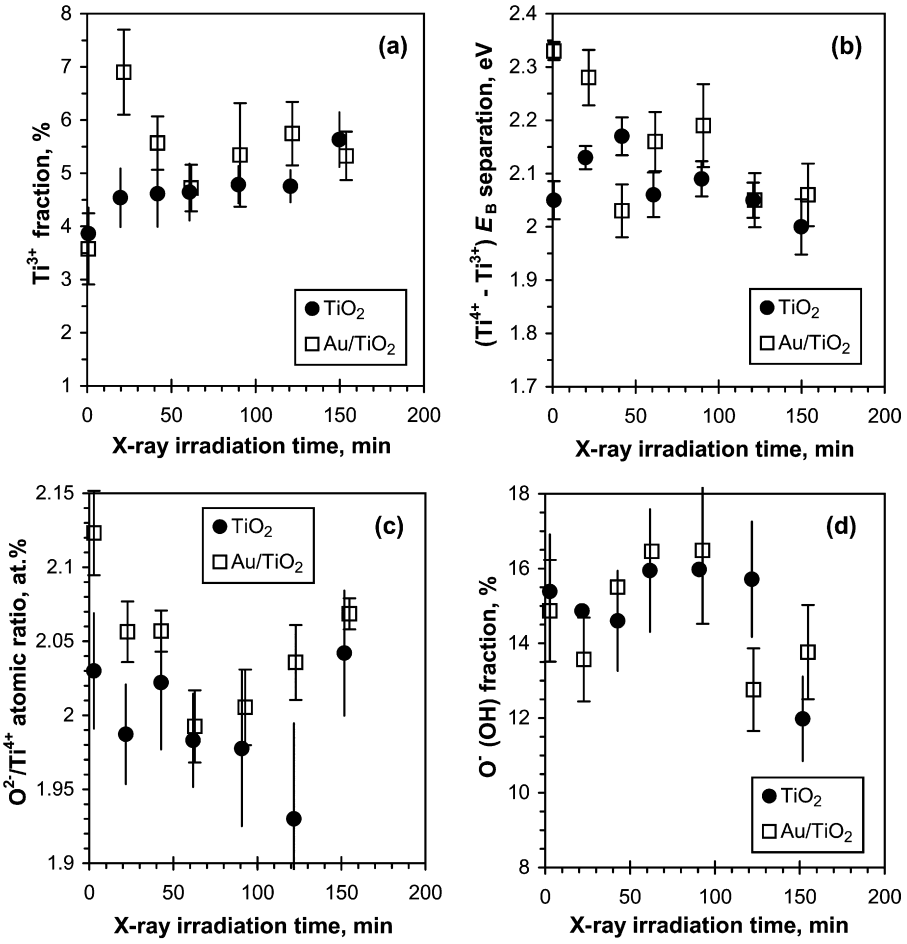

Fig. 6. X-ray induced changes in anatase TiO_2 (filled circles) and Au/TiO_2 catalyst (squares): (a) fraction of reduced Ti^{3+} species, (b) energy separation between Ti^{4+} and Ti^{3+} peaks, (c) O^{2-}/Ti^{4+} atomic ratio, and (d) fraction of high-energy component (O^-, OH^- species) in the O 1s spectrum as a function of X-ray irradiation time.

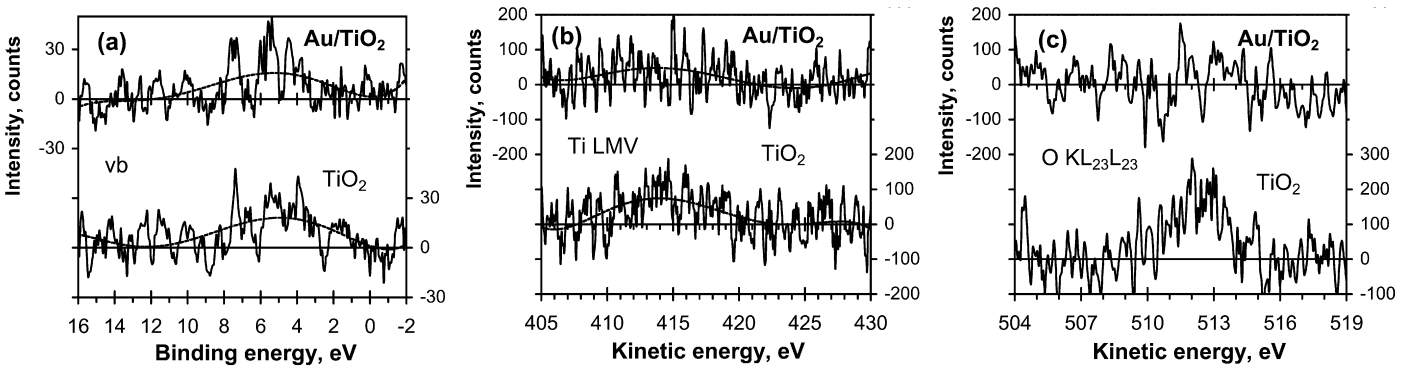

Fig. 7. Difference spectra showing changes in (a) valence band, (b) Ti LMV and (c) O KLL Auger peaks of TiO_2 and of Au/TiO_2 catalyst after X-ray irradiation for 160 min relative to virgin samples.

present in the virgin Au/TiO_2 grows rapidly at the beginning of X-ray irradiation before remaining nearly constant for the rest of the time. In the WGC catalyst, the fraction of the Ti^{3+} species seems to be steadily larger than in TiO_2 (Fig. 6(a)). Note that a similar increase in the Ti^{3+} fraction during the initial stage of X-ray irradiation (0–50 min) was observed in the in-house Au/TiO_2 catalyst as well. A larger energy separation between the Ti^{4+} and Ti^{3+} peaks observed in the Ti 2p spectra of Au/TiO_2 as compared to TiO_2 in the initial stage of X-ray irradiation also implies a higher extent of reduction of titanium in the former sample (Fig. 6(b)). In both samples, the O^{2-}/Ti^{4+} atomic ratio decreases during the ongoing X-ray irradiation and passes through a minimum after irradiation for 60–100 min before recovering (Fig. 6(c)). The fraction of the high-energy O 1s component (O^-, OH species) also changes non-monotonically, attaining in both samples a maximum after irradiation for 60–100 min (Fig. 6(d)).

X-rays also cause some alterations in the valence band of the samples. This becomes obvious in the difference spectra obtained by subtracting the valence band spectrum of the virgin sample from that acquired at the end of the experiment (t_{irr} = 160 min). Fig. 7(a) reveals for TiO_2 an intensity enhancement in the binding energy range of 1–8 eV along with a broad maximum at ~5 eV. This seems to be associated with an increasing contribution of O 2p non-bonding orbitals in the electronic structure of irradiated anatase. A similar difference spectrum is observed for the WGC catalyst (Fig. 7(a), Au/TiO_2).

The Ti LMV Auger difference spectrum of the irradiated TiO_2 sample shows a higher intensity in the kinetic energy region of 410–420 eV (Fig. 7(b)). This implies that Ti LMV transitions benefit from the enhanced density of valence band states induced by X-rays (see Fig. 7(a), TiO_2). The irradiation effect in TiO_2 is even more pronounced for the O KVV Auger peak. This is demonstrated by an intense band centered at ~512.5 eV in the difference spectrum (Fig. 7(c), TiO_2), which seems to be mainly related to non-bonding O 2p states. By contrast, no appreciable (or rather faint) irradiation effects are observed for the Ti LMV (Fig. 7(b), Au/TiO_2) and O KVV (Fig. 7(c), Au/TiO_2) Auger peaks of the WGC catalyst. It should be noted that the valence band and Auger spectra of the samples defined as "virgin" are actually taken after ~12–18 min of X-ray irradiation. At this point in time some changes in the structure and composition have already occurred (Figs. 3–6). Therefore, the actual X-ray damage is probably larger than that indicated in the difference spectra of Fig. 7.

X-ray irradiation of the samples is also observed to be accompanied by gas release. A sharp rise of the background pressure in the analytical chamber is seen once irradiation begins. According to Fig. 8(a), the initial pressure jump is stronger for TiO_2 than for the WGC catalyst. Evolution of oxygen from the samples during X-ray irradiation monitored by a quadrupole mass spectrometer (ion peak $^{16}O^+$) is shown in Fig. 8(b). It appears that the initial spike in the $^{16}O^+$ emission is caused by the removal of adsorbed oxygen and hydroxyl groups. On the other hand, the slowly descending part of the $^{16}O^+$ evolution curve seems to be associated with the removal of lattice oxygen atoms from surface layers. The data indicate that oxygen desorption from the WGC catalyst is lower than that from

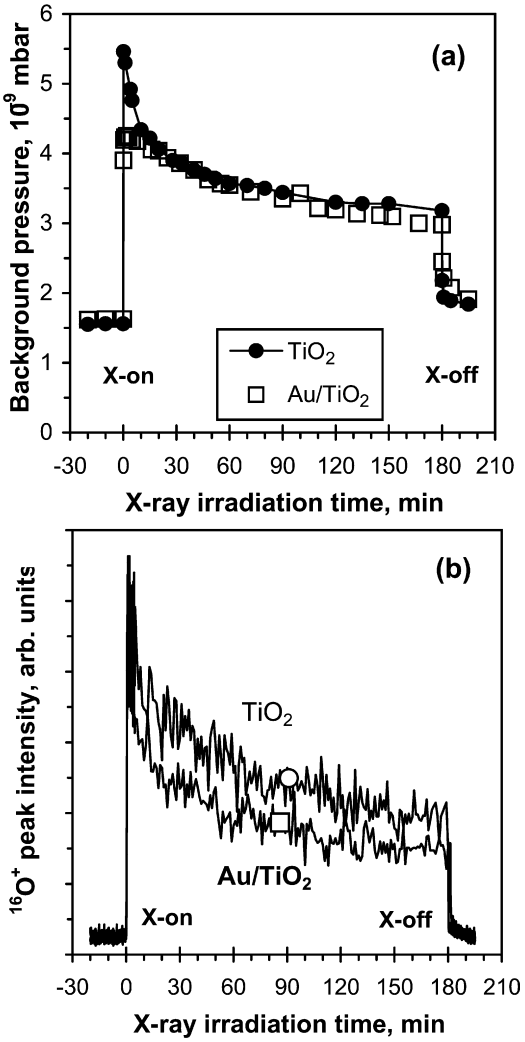

Fig. 8. Variation of (a) background pressure in the analytical chamber and of (b) intensity of oxygen ion peak in the residual gas mass spectrum as a function of time of exposure to X-rays for anatase TiO_2 (circles) and Au/TiO_2 catalyst (squares).

TiO_2 (Fig. 8(b)). Termination of X-ray irradiation causes an abrupt drop in the background pressure and in the $^{16}O^+$ signal (Fig. 8). No change in the $^{28}CO^+$ and $^{44}CO_2{}^+$ emission intensity caused by X-ray irradiation is observed. Note that any possible effects of sample temperature rise due to the X-rays on the data presented in Fig. 8 can be excluded. Actually, after 80–90 min of X-ray irradiation the temperature at the surface of the samples, which was monitored with a Ni–NiCr thermocouple pressed into the powder layer, reached a stable level of only ~35 °C, with the overall temperature elevation amounting to about 10 °C.

4. Discussion

This paper focuses on two issues considered to be key in evaluating XPS data for Au/TiO_2 catalysts: (i) the electronic state of gold surface atoms and (ii) the effect of extended X-ray irradiation of samples. We first turn to the XPS-based discussion of the Au oxidation state in Au/TiO_2 catalysts for which the correct measurement of the Au $4f_{7/2}$ binding energy is of pivotal importance. Generally, the problem of determining accurate binding energies in a system of nano-sized particles on an insulating support is complicated by charging effects and therefore crucially dependent on reliable referencing.

The most commonly employed technique of energy referencing in XPS characterization of supported catalysts is the use of the C 1s peak attributed to "adventitious" surface carbon. The procedure assumes that (i) the differential charging is negligible so that the entire spectrum is uniformly shifted by a constant energy due to integral sample charging and (ii) the C 1s line of adventitious carbon is independent of the chemical heterogeneity of the sample. Yet there are many factors that can affect the measured C 1s binding energy of a carbon contamination layer, e.g., the chemical state of the carbon, the thickness of the contamination layer, the chemical and physical nature of the substrate and so forth [50]. We observe the C 1s line in the Au/TiO_2 WGC catalyst to be shifted to higher binding energies by ~0.27 eV relative to that in the reference TiO_2 anatase and, in addition, to have a different shape. Note that a higher value of the C 1s E_B in Au/TiO_2 as compared to TiO_2 is not characteristic of the WGC catalyst solely. In the in-house Au/TiO_2 catalysts prepared by deposition–precipitation of gold onto a home-made anatase precursor [45], the C 1s E_B is also larger by 0.15–0.2 eV than that in TiO_2. This means that charging effects in both samples cannot be properly corrected by the same procedure of referencing to the C 1s line. Besides, because of the low intensity of the C 1s peak in catalysts, its reliable deconvolution and, accordingly, the accurate determination of E_B become problematic (cf. error bars in Figs. 4(a), (c) and 5(a), (b)).

Alternatively, binding energies may be referenced to the main peaks of the support, in particular to the Ti $2p_{3/2}$ E_B [8,12], O 1s E_B [22] or Ti 3p line [51]. It should be noted, however, that the correct determination of the Au $4f_{7/2}$ binding energy depends on both the choice of the proper reference line and on the actual reference value as well. Besides, in view of the obtained results, a possible dependence of the support core-level binding energy on X-ray irradiation exposure should be taken into account.

In XPS studies of Au/TiO_2 catalysts the C 1s and Ti $2p_{2/3}$ E_B reference values are typically taken from literature data. They range from 284.5 eV [24] to 285.0 eV [10,15,17,26] for C 1s (with the latter value being most frequently used) and from 458.8 eV [8] to 459.2 eV [12] for Ti $2p_{3/2}$. In the present work, the reference values are obtained *in situ* by measuring the C 1s E_B = 284.8 eV on air-exposed polycrystalline Ag and Au $4f_{7/2}$ E_B = 84.01 eV on sputter-cleaned Au foil. Using the C 1s peak of aliphatic carbon as a reference, we find for TiO_2 the charge-corrected Ti $2p_{3/2}$ and O 1s binding energies to be 458.85 eV (Ti^{4+}) and 530.01 eV (O^{2-}), respectively, which are typical for titania [39,41,52]. In the Au/TiO_2 WGC catalyst, the derived Au $4f_{7/2}$ binding energy is 83.55 eV if charge correction is introduced via the C 1s line in the catalyst; if the C 1s line in TiO_2 is considered to be a proper reference for charge correction, Au $4f_{7/2}$ E_B = 83.85 eV. Using the charge-corrected Ti $2p_{3/2}$ and O 1s binding energies in TiO_2 as references, one can arrive at values of 83.8 eV and, respectively, 83.72 eV for Au $4f_{7/2}$ E_B. Finally, taking the Ti 3p E_B = 37.5 eV as a reference, we obtain Au $4f_{7/2}$ E_B = 83.66 eV. By applying the same correction procedure to the in-house Au/TiO_2 catalyst, which shows a very similar CO oxidation performance (CO conversion of 88% [45]) as that of the WGC standard, we found the Au $4f_{7/2}$ E_B to be in the range 83.6–83.8 eV. Thus, the accurate determination of the Au $4f_{7/2}$ binding energy in Au/TiO_2 catalysts is an obvious problem. Note, however, that for any means of correction the Au $4f_{7/2}$ binding energy in Au/TiO_2 is in the range of 83.55–83.85 eV and thus always lower than that in pure Au foil.

A decrease in the Au $4f_{7/2}$ binding energy for Au/TiO_2 catalysts relative to that in bulk Au was observed in a number of studies [8,13–17,24,26–28,30]. The reported negative shifts of the Au $4f_{7/2}$ E_B are scattered in a wide range from −0.2 to −1.2 eV. Zwijnenburg et al. [14] explained such a negative shift of the Au $4f_{7/2}$ binding energy by final state effects associated with a reduced screening of core holes in an assembly of low-coordinated gold surface atoms. Radnik et al. [8] considered the reduced coordination number of Au atoms as the main reason of the negative binding energy shift and related it to the degree of rounding of Au nanoparticles which is dependent on the particle–support interaction. In addition, the authors did not exclude the process of electron transfer from the support to the Au particle as a possible contribution to the decrease of the Au $4f_{7/2}$ E_B. Arrii et al. [26] have further developed the idea that particle–support interactions play a decisive role. They suggested that the shift of the Au $4f_{7/2}$ peak towards lower E_B can be better explained by an initial state effect associated with electron transfer from Ti^{3+} surface defect states to Au clusters.

Theoretical studies [53,54] have shown that the deposition of Au nanoparticles on a reduced rutile TiO_2 (1 1 0) surface should result in a strong adsorption of Au on oxygen vacancies (bridging sites) since the excess electron density in these sites can be donated to gold atoms. Indeed, for Au nanoclusters deposited on a TiO_2 (1 1 0) surface containing a large concentration of oxygen vacancy defects, the Au $4f_{7/2}$ E_B was observed to be lower than that for Au deposited on TiO_2 either stoichiometric [55] or of low defectiveness [46]. Based on these considerations we envisage a similar scenario of electron transfer from $Ti^{\delta+}$ related sites to Au nanoparticles in both WGC and in-house Au/TiO_2 catalysts. The deconvolution of the Ti 2p spectrum has provided clear evidence for the presence of a certain concentration of Ti oxidation states lower than +4 (see Fig. 1(a)) in both Au/TiO_2 catalysts. Such states are inevitably associated with oxygen vacancies. The idea of charge transfer is also supported by a shift of the Ti 2p peak to lower binding energies in intact Au/TiO_2 with respect to that in TiO_2 (Fig. 5(a)) and by an enhanced contribution of O 2p non-bonding orbitals to the valence band of Au/TiO_2 (Fig. 2(d)). The charge transfer from electron-rich O-vacancies to Au atoms is also corroborated by a larger E_B of the high-energy OII component (O^-, OH^-) in the O 1s spectrum of Au/TiO_2 as compared to TiO_2, assuming the OII species to represent mainly low-coordinated $O^{\delta-}$ atoms and oxygen vacancies.

According to density-functional theory calculations [56], the interaction between gold and a TiO_2 surface containing oxygen vacancies results in a local perturbation of the electronic structure causing a shift in the density of states as compared to bulk Au or to Au atoms adsorbed on a perfect TiO_2 surface. It is also shown that in case of adhesion of gold on an oxygen vacancy the electrons are accumulated between the gold and the two titanium atoms next to the vacancy, and that the bond is covalent. Such localization of electrons may bring about a modification of the Ti–O bonds and a

decrease in their ionicity that may be responsible for the negative shift of the correct Ti 2p E_B of about 0.12 eV observed in Au/TiO_2 relative to that in TiO_2 (Fig. 5(a)). Redistribution of the Ti–O bonds in the presence of Au particles is also indirectly indicated by an enhanced contribution of the O 2p non-bonding states to the O KVV Auger transition in the Au/TiO_2 catalyst as compared to TiO_2 (Fig. 2(f)).

We now turn to the observation of sample damage during extended X-ray exposure. The irradiation of Au/TiO_2 and TiO_2 produces multiple-hole states in the valence band of the samples as a result of electron–hole pair generation and Auger decay processes [5]. The arising charging of the samples is seen to cause a slight gradual broadening of the Ti 2p peak (Fig. 3(a)) and the shift of the Ti 2p and O 1s peaks to higher binding energies (Figs. 3(b) and (c)). Multiple holes in the valence band break bonds between Ti and O atoms which results in the reduction of the titanium oxidation state (Fig. 6(a)) along with the desorption of oxygen (Fig. 8(b)). Thus structural changes must be encountered which may lead to rehybridization between O 2p non-bonding orbitals and Ti 3d/4s states in titania [57]. As can be seen from Fig. 7(a), the change in the electronic structure of irradiated TiO_2 is clearly evidenced by an enhanced occupation of the O 2p non-bonding states in the valence band and their involvement in the O KVV Auger transition (Fig. 7(c), TiO_2). Hence X-ray induced structural/chemical modifications extend at least to the depth sampled by the O 2p electrons.

X-ray induced desorption of oxygen from the samples is accompanied by a diminution of the O^{2-}/Ti^{4+} atomic ratio (Fig. 6(c)). After X-ray irradiation for 60–100 min the relative change of stoichiometry of the support in Au/TiO_2 appears to be slightly larger than in TiO_2 (~5.7% and 3%, respectively). The non-monotonic variation of the O^{2-}/Ti^{4+} ratio seems to result from the competition of two processes, namely the ejection of oxygen atoms from surface layers and the diffusion of oxygen atoms from the bulk into the defect region. The variation of the fraction of OII species in TiO_2 and in Au/TiO_2 under X-ray irradiation which is inverse to the change of the O^{2-}/Ti^{4+} ratios in these samples (cf. Fig. 6(c) and (d)) implies that these OII species represent mainly the $O^{\delta-}$ ions and O-vacancies. The opposite variation of the energy separation between the Ti^{4+} and Ti^{3+} peaks for TiO_2 and Au/TiO_2 WGC in the initial stage of X-ray irradiation (Fig. 6(b)) suggests that damaging processes in the samples develop differently.

The removal of oxygen atoms from the TiO_2 surface leaving behind electron-rich vacancies causes charge redistribution in the system which extends to regions far from the vacancy site. This results in substantial alterations in the positions of the remaining atoms [53] which should affect both the local charge and the Madelung energy of a particular atom. The variation of charge-corrected core-level binding energies in the X-ray irradiated Au/TiO_2 WGC catalyst and TiO_2 (Figs. 4 and 5) shows that the charge and atoms redistribution processes proceed in these samples in a different way. In TiO_2, X-ray irradiation has practically no effect on the binding energy of the components or brings about a slight shift of the Ti 2p (Ti^{4+} species) and O 1s, O 2s (O^{2-} species) lines to a lower E_B (Figs. 4(d) and 5(a), (b)). On the contrary, the binding energies of the Ti $2p_{3/2}$ and O 2s peaks in Au/TiO_2 WGC steadily increase (Fig. 4).

Note that X-ray irradiation of the Au/TiO_2 WGC catalyst for 10–50 min is accompanied by a decrease in the Au $4f_{7/2}$ E_B (Fig. 5(c)) which indicates that electrons are donated to Au atoms due to the generation of additional reduced Ti^{3+} species [26,53]. Accordingly, a consistent rise of the Ti^{3+} fraction in Au/TiO_2 in this X-ray exposure range is observed (Fig. 6(a)). Obviously, this charge transfer involves only atoms at the Au–TiO_2 interface, so that the charge state of Ti atoms in deeper layers remains practically unaffected (see Fig. 4(b), Ti 3p data). Further X-ray irradiation of Au/TiO_2 causes a gradual rise of the Au $4f_{7/2}$ E_B (Fig. 5(c)) which may be explained by a competitive process of electron charge transfer from Au to fill the photoholes in the valence band and to compensate for the electron deficiency in the O-vacancy sites at the surface. Additionally, an increase in the Au $4f_{7/2}$ E_B and a decrease in the Au $4f_{7/2}$ FWHM at higher X-ray exposures may also be associated with some irradiation-induced annealing of Au/TiO_2 which would result in the Au nanoparticles being more spherical and homogeneous in size distribution [21]. Thus, the drop in the Au $4f_{7/2}$ E_B and the increase in the Ti^{3+} fraction in the Au/TiO_2 catalysts provide the direct evidence for the charge transfer from the oxygen vacancies created in the TiO_2 support by X-ray irradiation to Au nanoparticles. This observation can be compared with a recent XPS study of Au clusters deposited on stoichiometric and reduced rutile TiO_2 (1 1 0) surface reported by Jiang et al. [23] who revealed that the charge transfer to Au particles occurs only from the reduced TiO_2 surface. The negative shift of the Au $4f_{7/2}$ E_B by 0.07 eV measured in this work [23] and caused by electron transfer to Au clusters strongly corroborates our findings.

5. Summary

This XPS study has revealed a number of features in the electronic structure of Au/TiO_2 catalysts as compared to TiO_2 (anatase). The valence band of Au/TiO_2 shows the presence of Au 5d bands and an enhanced contribution of the O 2p non-bonding states while it is otherwise largely TiO_2-like. Interaction of Au particles with the support seems to affect the Ti–O bonds at the surface which results in a lower Ti 2p binding energy in an intact Au/TiO_2 as compared to that in TiO_2. Au nano-sized particles in the catalyst are slightly negatively charged due to the electron transfer from oxygen vacancies of the support, so that the charge-corrected Au $4f_{7/2}$ core-level binding energy in Au/TiO_2 is 0.15–0.45 eV lower than that in pure bulk Au. The shape and the energy position of the C 1s line in the Au/TiO_2 catalysts are found to be noticeably different from those in TiO_2, and therefore using the C 1s core level for accurate energy referencing and determining the chemical state of gold particles in case of Au/TiO_2 catalysts appears questionable. Instead, referencing to corrected core-level lines of the support which are not influenced by X-ray irradiation is preferable.

Exposure of Au/TiO_2 catalysts and TiO_2 to X-rays gives rise to Ti–O bond breaking, reduction of the Ti^{4+} state and desorption of oxygen from surface layers. As a result, changes in the surface composition and electronic structure of the samples develop with time. This is indicated by an increase in the fraction of Ti^{3+} species, a non-monotonic diminution of the O^{2-}/Ti^{4+} atomic ratio, the modification of the valence band and the variation of core binding energies. It is worth noting that the pattern of X-ray induced damage in the Au/TiO_2 catalyst is quite different from that in TiO_2, with some characteristics varying in an opposite way. While Ti 2p and O 1s binding energies in TiO_2 remain practically unaffected under extended X-ray irradiation, in Au/TiO_2 a gradual increase in the Ti 2p binding energy with X-ray exposure is observed. Actually, calcined Au/TiO_2 catalysts and TiO_2 turn out to be relatively resistant to X-ray irradiation: the maximum change of the core binding energy does not exceed 0.12 eV, with stabilization of the Ti 2p and Au 4f binding energies being attained after 75–95 min of X-ray irradiation. Though the effects of X-ray irradiation in Au/TiO_2 catalysts are rather small, they provide the direct evidence for charge transfer processes in this system triggered by production of oxygen vacancies in the support.

Acknowledgements

N.K. acknowledges support by ARC of the Communauté Francaise de Belgique and by COST D36 of the EC. A partial financial

support of this work from the National Academy of Sciences of Ukraine in the framework of the Fundamental Research Program "Nanostructural Systems, Nanomaterials, Nanotechnologies-2008" is also acknowledged (S. Ch.).

References

[1] J.W. Niemantsverdriet, Spectroscopy in Catalysis, second ed., Wiley-VCH, Weinheim, 2000.
[2] E. Paparazzo, Surf. Sci. 234 (1990) L253–L258.
[3] Z. Zhang, V.E. Henrich, Surf. Sci. 321 (1994) 133–144.
[4] S.P. Chenakin, R. Prada Silvy, N. Kruse, Catal. Lett. 102 (2005) 39–43.
[5] S.P. Chenakin, R. Prada Silvy, N. Kruse, J. Phys. Chem. B 109 (2005) 14611–14618.
[6] J.M.C. Soares, P. Morrall, A. Crossley, P. Harris, M. Bowker, J. Catal. 219 (2003) 17–24.
[7] M.P. Casaletto, A. Longo, A. Martorana, A. Prestianni, A.M. Venezia, Surf. Interface Anal. 38 (2006) 215–218.
[8] J. Radnik, C. Mohr, P. Claus, Phys. Chem. Chem. Phys. 5 (2003) 172–177.
[9] N. Dimitratos, A. Villa, C.L. Bianchi, L. Prati, M. Makkee, Appl. Catal. A 311 (2006) 185–192.
[10] L.-H. Chang, N. Sasirekha, Y.-W. Chen, Catal. Commun. 8 (2007) 1702–1710.
[11] B. Schumacher, V. Plzak, M. Kinne, R.J. Behm, Catal. Lett. 89 (2003) 109–114.
[12] B. Schumacher, V. Plzak, J. Cai, R.J. Behm, Catal. Lett. 101 (2005) 215–224.
[13] J.H. Yang, J.D. Henao, M.C. Raphulu, Y. Wang, T. Caputo, A.J. Groszek, M.C. Kung, M.S. Scurrell, J.T. Miller, H.H. Kung, J. Phys. Chem. B 109 (2005) 10319–10326.
[14] A. Zwijnenburg, A. Goossens, W.G. Sloof, M.W.J. Craje, A.M. van der Kraan, L.J. de Jongh, M. Makkee, J.A. Moulijn, J. Phys. Chem. B 106 (2002) 9853–9862.
[15] F.W. Chang, H.Y. Yu, L.S. Roselin, H.C. Yang, T.C. Ou, Appl. Catal. A 302 (2006) 157–167.
[16] J. Huang, W.-L. Dai, H. Li, K. Fan, J. Catal. 252 (2007) 69–76.
[17] B. Tian, J. Zhang, T. Tong, F. Chen, Appl. Catal. B 79 (2008) 394–401.
[18] S. Shukla, S. Seal, Nanostruct. Mater. 11 (1999) 1181–1193.
[19] J.W. Sobczak, D. Andreeva, Stud. Surf. Sci. Catal. 130 (2000) 3303–3308.
[20] C.C. Chusuei, X. Lai, K. Luo, D.W. Goodman, Top. Catal. 14 (2001) 71–83.
[21] D. Dalacu, J.E. Klemberg-Sapieha, L. Martinu, Surf. Sci. 472 (2001) 33–40.
[22] B.R. Cuenya, S.-H. Baeck, T.F. Jaramillo, E.W. McFarland, J. Am. Chem. Soc. 125 (2003) 12928–12934.
[23] Z. Jiang, W. Zhang, L. Jin, X. Yang, F. Xu, J. Zhu, W. Huang, J. Phys. Chem. C 111 (2007) 12434–12439.
[24] G.M. Veith, A.R. Lupini, N.J. Dudney, J. Phys. Chem. C 113 (2009) 269–280.
[25] W.-S. Lee, B.-Z. Wan, C.-N. Kuo, W.-C. Lee, S. Cheng, Catal. Commun. 8 (2007) 1604–1608.
[26] S. Arrii, F. Morfin, A.J. Renouprez, J.L. Rousset, J. Am. Chem. Soc. 126 (2004) 1199–1205.
[27] P. Lignier, M. Comotti, F. Schüth, J.-L. Rousset, V. Caps, Catal. Today 141 (2009) 355–360.
[28] J.A. Moma, M.S. Scurrell, W.A. Jordaan, Top. Catal. 44 (2007) 167–172.
[29] S. Lee, C. Fan, T. Wu, S.L. Anderson, Surf. Sci. 578 (2005) 5–19.
[30] P. Konova, A. Naydenov, Cv. Venkov, D. Mehandjiev, D. Andreeva, T. Tabakova, J. Mol. Catal. A: Chem. 213 (2004) 235–240.
[31] T. Diemant, Z. Zhao, H. Rauscher, J. Bansmann, R.J. Behm, Top. Catal. 44 (2007) 83–93.
[32] V. Schwartz, D.R. Mullins, W. Yan, B. Chen, S. Dai, S.H. Overbury, J. Phys. Chem. B 108 (2004) 15782–15790.
[33] N. Weiher, E. Bus, L. Delannoy, C. Louis, D.E. Ramaker, J.T. Miller, J.A. van Bokhoven, J. Catal. 240 (2006) 100–107.
[34] R. Zanella, C. Louis, Catal. Today 107–108 (2005) 768–777.
[35] C.D. Wagner, W.M. Riggs, L.E. Davis, J.F. Moulder, G.E. Muilenberg (Eds.), Handbook of X-ray Photoelectron Spectroscopy, Perkin-Elmer, Minnesota, 1979.
[36] L. Zhang, R. Persaud, T.E. Madey, Phys. Rev. B 56 (1997) 10549–10557.
[37] F. Barrère, A. Lebugle, C.A. van Blitterswijk, K. de Groot, P. Layrolle, C. Rey, J. Mater. Sci.: Mater. Med. 14 (2003) 419–425.
[38] H. Liu, W. Yang, Y. Ma, Y. Cao, J. Yao, J. Zhang, T. Hu, Langmuir 19 (2003) 3001–3005.
[39] R. Sanjinés, H. Tang, H. Berger, F. Gozzo, G. Margaritondo, F. Lévy, J. Appl. Phys. 75 (1994) 2945–2951.
[40] A. Orendorz, J. Wüsten, C. Ziegler, H. Gnaser, Appl. Surf. Sci. 252 (2005) 85–88.
[41] J.-C. Dupin, D. Gonbeau, P. Vinatier, A. Levasseur, Phys. Chem. Chem. Phys. 2 (2000) 1319–1324.
[42] E. McCafferty, J.P. Wightman, Surf. Interface Anal. 26 (1998) 549–564.
[43] J.F. Porter, Y.-G. Li, C.K. Chan, J. Mater. Sci. 34 (1999) 1523–1531.
[44] G. Liu, Z. Chen, C. Dong, Y. Zhao, F. Li, G.Q. Lu, H.-M. Cheng, J. Phys. Chem. B 110 (2006) 20823–20828.
[45] S.P. Chenakin, A. Bongiovanni, M.A. Vasylyev, I.N. Makeeva, N. Kruse, Metallofiz. Noveishie Technol. 31 (2009) 589–602.
[46] A. Howard, D.N.S. Clark, C.E.J. Mitchell, R.G. Egdell, V.R. Dhanak, Surf. Sci. 518 (2002) 210–224.
[47] P. Le Fèvre, J. Danger, H. Magnan, D. Chandesris, J. Jupille, S. Bourgeois, M.-A. Arrio, R. Gotter, A. Verdini, A. Morgante, Phys. Rev. B 69 (2004) 155421-1–155421-9.
[48] A. von Richthofen, R. Cremer, R. Domnick, D. Neuschütz, Thin Solid Films 315 (1998) 66–71.
[49] J. Riga, C. Tenret-Noel, J.J. Pireaux, R. Caudano, J.J. Verbist, Y. Gobillon, Phys. Scripta 16 (1977) 351–354.
[50] P. Swift, Surf. Interface Anal. 4 (1982) 47–51.
[51] E.A. Willneff, S. Brown, D. Rosenthal, H. Bluhm, M. Hävecker, E. Kleimenov, A. Knop-Gericke, R. Schlögl, S.L.M. Schroeder, J. Am. Chem. Soc. 128 (2006) 12052–12053.
[52] J.E. Gonçalves, S.C. Castro, A.Y. Ramos, M.C.M. Alves, Y. Gushikem, J. Electron. Spectrosc. Relat. Phenom. 114–116 (2001) 307–311.
[53] A. Vijay, G. Mills, H. Metiu, J. Chem. Phys. 118 (2003) 6536–6551.
[54] K. Okazaki, S. Ichikawa, Y. Maeda, M. Haruta, M. Kohyama, Appl. Catal. A 291 (2005) 45–54.
[55] T. Okazawa, M. Kohyama, Y. Kido, Surf. Sci. 600 (2006) 4430–4437.
[56] N. Lopez, J.K. Nørskov, T.V.W. Janssens, A. Carlsson, A. Puig-Molina, B.S. Clausen, J.-D. Grunwaldt, J. Catal. 225 (2004) 86–94.
[57] A.G. Thomas, W.R. Flavell, A.R. Kumarasinghe, A.K. Mallick, D. Tsoutsou, G.C. Smith, R. Stockbauer, S. Patel, M. Grätzel, R. Hengerer, Phys. Rev. B 67 (2003) 035110-1–035110-7.